Thin Films of Solvatomagnetic CN-Bridged Coordination Polymers: From Micro to Nanoscale

Aleksandra Pacanowska, Magdalena Fitta,* Marcin Kozieł, and Beata Nowicka*

Two types of thin films differing in thickness and morphology of microporous CN-bridged hybrid organic–inorganic $\{[Ni^{II}(cyclam)]_3[M^{III}(CN)_6]_2 \cdot nH_2O\}n$ (M = Cr or Fe, cyclam = 1,4,7,11-tetraazacyclotetradecane) coordination networks are obtained by using physical and chemical deposition techniques. By adsorption on the PET/ITO substrate of the pre-formed nano-sized crystallites from water suspension, films of 1–2 μm thickness composed of 40–200 nm size particles are obtained. The use of chemical sequential growth method, in which the coordination framework is anchored to the gold surface and built directly on the substrate from the cationic and anionic building blocks, reduces the film thickness to 100 nm and drastically improves film morphology. Both types of thin films show solvatomagnetic behavior characteristic for bulk compounds and change magnetic characteristics, including the shape of the magnetic hysteresis, under different humidity conditions.

1. Introduction

Molecule-based magnets offer an interesting alternative to classical materials in the development of modern technologies.[1] Their construction, based on molecular fragments combined into intricate architectures, allows merging at the molecular level a range of desirable properties, including magnetic ordering,[2] porosity and sorption,[3] bistability,[4] and sensitivity to external stimuli, such as temperature,[5] pressure,[6] light[7] or presence of small molecules[8] Solvatomagnetic effect or magnetic sponge-like behavior, defined as reversible changes in structure and magnetic characteristics upon sorption of small guest molecules,[9] is one of the remarkable features that can be employed in the design of sorption-driven magnetic sensors and switches.[10,11]

A. Pacanowska, M. Fitta
Institute of Nuclear Physics Polish Academy of Sciences
Radzikowskiego 152, Kraków 31-342, Poland
E-mail: magdalena.fitta@ifj.edu.pl
A. Pacanowska, M. Kozieł, B. Nowicka
Faculty of Chemistry
Jagiellonian University
Gronostajowa 2, Kraków 30-387, Poland
E-mail: beata.nowicka@uj.edu.pl

Cyano-bridged coordination polymers constitute an important group of molecule-based magnets.[12–14] The CN-bridges mediate relatively strong magnetic interactions and at the same time they allow reasonable control over the self-assembly process and thus the rational design of versatile topologies by the use of appropriate blocking ligands. Moreover, the CN-bridges are robust but bendable, which may give rise to framework flexibility and structural transformations triggered by desolvation or sorption of small molecules. Since the sign and magnitude of magnetic superexchange for many metal ions depend on the geometry of the CN-bridges, the structurally flexible networks often show sorption-driven changes in magnetic characteristics. Porosity is not common in CN-bridged polymers, since the CN-ligands are relatively short. However, it can be introduced by the use of additional long organic bridging ligands or pre-defined complex building blocks acting as linear linkers. Following the later approach, by using Ni^{II} with equatorial positions blocked by the cyclam ligand (cyclam = 1,4,7,11-tetraazacyclotetradecane), a family of microporous 2D networks of characteristic honeycomb-like topology, based on hexa- or octa-cyanometallates have been obtained.[15–17] Although these coordination polymers do not contain any coordinated solvent molecules, they show unusually rich solvatomagnetic effect, connected with sorption of guest solvent molecules, like water or methanol, into the microporous channels. The structural transformations upon guest inclusion are restricted to changes in bond geometry and the deformation of the coordination skeleton, which retains its original topology. However, even these relatively small structural changes cause marked differences in magnetic properties between different pseudopolymorphic forms.[18] Two isostructural $\{[Ni^{II}(cyclam)]_3[M^{III}(CN)_6]_2 \cdot nH_2O\}n$ (M = Cr or Fe) networks proved to be particularly robust and were characterized as two different hydrates and an anhydrous form, with fully reversible interconversion pathways between them.[19] In view of potential applications of the solvatomagnetic effect we decided to find effective methods of surface deposition for the above mentioned networks and investigate if their properties are retained in thin films.

Preparation of molecule-based magnetic materials in the form of thin films is an important step toward exploration of their application potential.[20] Compounds in the form of thin films react more efficiently to external stimuli and are more suitable for the construction of molecular devices. Several

**ADVANCED
SCIENCE NEWS**

www.advancedsciencenews.com

**ADVANCED
MATERIALS
INTERFACES**

www.advmatinterfaces.de

methods have been employed for the preparation of thin films of molecular magnetic materials, depending on their structure and properties of the building blocks. They include Langmuir–Blodgett technique,[21–23] electrodeposition,[24–26] chemical vapor deposition[27,28] as well as spin- and dip-coating methods.[29] The studies of surface-deposition of molecule-based magnetic materials focused on three groups of functional systems: single molecule magnets (SMM),[30,31] photomagnets,[32–34] and materials with long range magnetic ordering, especially those with relatively high T_c values.[26,35,36] The research into the thin film formation of cyano-bridged networks concentrated almost exclusively on Prussian Blue Analogues (PBAs),[37] which are purely inorganic coordination polymers of regular cubic structure. Deposition of hybrid organic–inorganic CN-bridged networks, apart from isolated reports, is a practically unexplored area.[38–41] Numerous earlier studies on other molecular magnets, particularly those devoted to anchoring SMMs on surfaces, have shown that magnetic properties are easily influenced by both reduction of the particle size as well as interface interactions with the substrate.[42–44] Therefore, in order to employ solvatomagnetic properties in the construction of chemo-sensitive switches it is essential to investigate if the properties of the bulk material are retained in thin films. To the best of our knowledge there are no reports on the solvatomagnetic effect in thin films. The aim of our work was to obtain uniform and robust films, which react to changes in humidity by changes in magnetic properties. In this report we present the preparation and magnetic studies of two types of thin films of the $\{[Ni^{II}(cyclam)]_3[M^{III}(CN)_6]_2 \cdot nH_2O\}n$ (M = Cr or Fe) networks: micrometric-sized films obtained by physical deposition and nanometric-sized films obtained by chemical deposition.

2. Results and Discussion

2.1. Deposition and Film Morphology

Uniform thin films of the studied compounds can be obtained by physical or chemical deposition methods. In the physical deposition method the nanocrystallites of the coordination polymers were deposited on the substrate from water suspension in the dip-coating process. In the chemical deposition method of sequential growth the networks were formed directly on the substrate surface from anionic and cationic building blocks.

The $\{[Ni^{II}(cyclam)]_3[Cr^{III}(CN)_6]_2 \cdot nH_2O\}_n$ (NiCr) and $\{[Ni^{II}(cyclam)]_3[Fe^{III}(CN)_6]_2 \cdot nH_2O\}_n$ (NiFe) networks are easily obtained in water solution reactions. Due to high lability of the Ni^{II} cations the formation of CN-bridges is instantaneous and upon mixing of appropriate building blocks the networks precipitate immediately in the form of a fine powder. Therefore, the first method of film formation we decided to employ was the deposition of pre-formed nano-sized crystallites from water suspension by dip-coating. The PET/ITO foil modified by poly(diallyldimethylammonium chloride) (PDADMAC), in order to increase hydrophilicity, was chosen as the most suitable substrate, providing good adhesion, favorable mechanical properties, as well as low mass and therefore low diamagnetic contribution in the magnetometric measurements. Single dip-coating cycle consisted of 30 s immersion in constantly stirred water suspension of the compound followed by 30 s drying in air. 25 cycles gave full coverage of the substrate with a uniform film of 1–2 µm thickness. The SEM images (**Figure 1**) show that the deposited crystallites have the form of hexagonal blocks with well-defined edges and vary in size in the range of 30–200 nm, with the average size slightly larger for the NiCr network
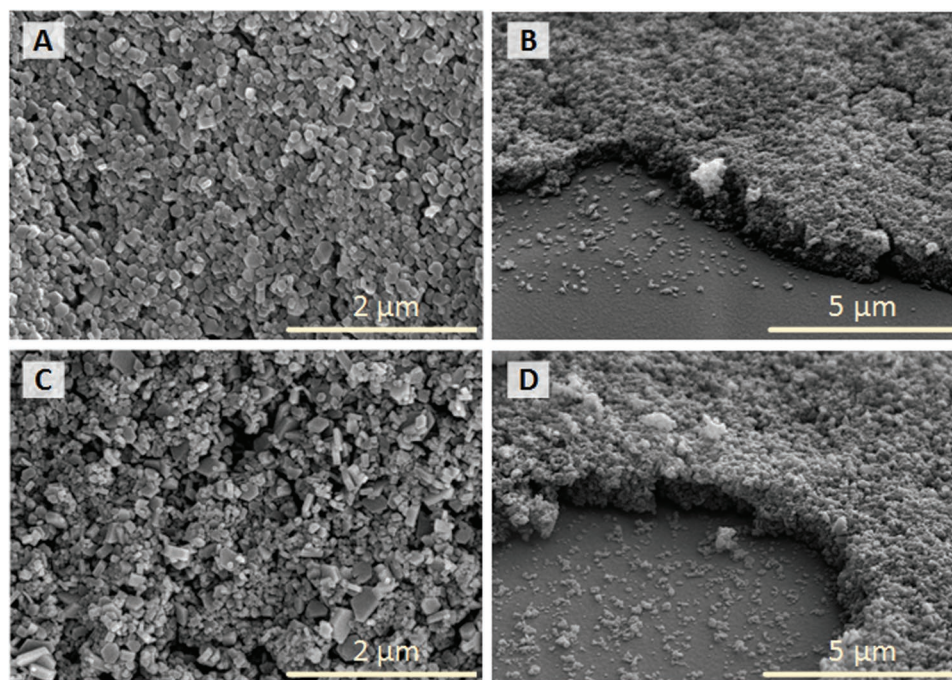

Figure 1. Top view (left) and 45°-tilted (right) SEM images of films fabricated by dip-coating from suspension for A,B) $\{[Ni^{II}(cyclam)]_3[Cr^{III}(CN)_6]_2 \cdot nH_2O\}_n$ and C,D) $\{[Ni^{II}(cyclam)]_3[Fe^{III}(CN)_6]_2 \cdot nH_2O\}_n$.

2201834 (2 of 9)

**ADVANCED
SCIENCE NEWS**

www.advancedsciencenews.com

**ADVANCED
MATERIALS
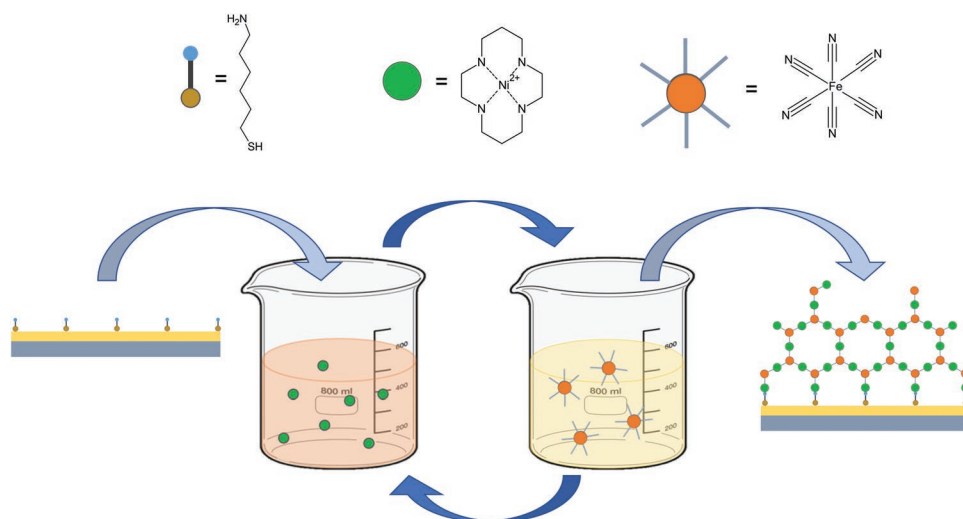INTERFACES**

www.advmatinterfaces.de

Figure 2. Schematic representation of the coordination network assembly directly on the substrate surface through the formation of CN-bridges.

(80 nm) than for the NiFe network (60 nm) (Figure S1, Supporting Information). The particles are loosely packed, which results in a slightly rough surface, but without visible fissures or flaws. The thickness of the films can be increased by additional dip coating cycles, but not decreased below 1 μm, since the lower number of cycles results in incomplete surface coverage.

The second method of film deposition that we used was sequential growth. Modeled after layer-by-layer method it is well suited for deposition of coordination polymers and was successfully used to construct thin films of PBAs.[45,46] Initially the cationic building block was anchored by 6-aminohexanethiol to the surface of gold-spattered PET/ITO foil. Then the substrate was sequentially immersed in water solutions of the building blocks: $K_3[M(CN)_6]$ and $[Ni(cyclam)](NO_3)_2$. During this process the coordination network is assembled directly on the substrate surface through the formation of the CN-bridges (**Figure 2** and Figure S2, Supporting Information). Thorough rinsing in water was applied between the immersions in order to prevent mixing of the building blocks solutions and precipitation of the bulk compound. The deposition process comprised 500 cycles. The resulting films surface (**Figure 3**) is composed of closely packed round-shaped grains of 20–30 nm, much smaller than the crystallites deposited from suspension. The grains are molded together and show very narrow size distribution
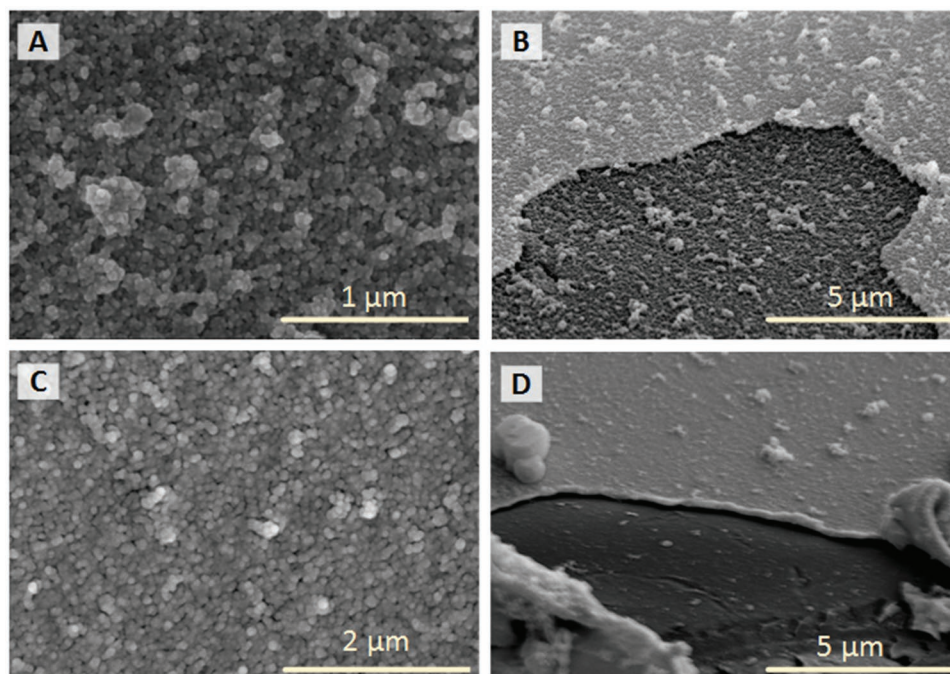

Figure 3. Top view (left) and 45°-tilted (right) SEM images of films obtained by sequential growth for A,B) $\{[Ni^{II}(cyclam)]_3[Cr^{III}(CN)_6]_2 \cdot nH_2O\}_n$ and C,D) $\{[Ni^{II}(cyclam)]_3[Fe^{III}(CN)_6]_2 \cdot nH_2O\}_n$.

**ADVANCED
SCIENCE NEWS**

www.advancedsciencenews.com

**ADVANCED
MATERIALS
INTERFACES**

www.advmatinterfaces.de

(Figure S1, Supporting Information), which results in much lower roughness of the surface in comparison to the films obtained from suspension. The thickness of the layers is about 100 nm, which is 10 times less than in the physical deposition method. Increased number of cycles resulted in the appearance of numerous microcrystallites on the film surface. We did not attempt experiments with less than 500 cycles to achieve lower film thickness, since the magnetic signal of the 100 nm thick films was already very weak (see Section 2.3).

The films microstructure compares favorably to that of the films obtained from related CN-bridged networks. The films obtained from suspension show smaller grain size and better surface evenness in comparison to PBAs obtained by electrochemical deposition,[24] the Fe^{II}-Nb^{IV} based network obtained by ion-exchange[41] and the Fe^{II}-Pt^{II} Hoffman-type network obtained by pulsed laser evaporation.[38] The morphology of the films obtained by sequential growth is similar to that of the films obtained by the same method from PBAs[33] and Hoffman-type networks.[40]

We attempted further structural characterization of the films by powder x-ray diffraction (PXRD). However, due to small amount of the deposited material no peaks related to the coordination network were observed for the nanometric films obtained by the sequential growth method. In the case of the micrometric films obtained from suspension the PXRD experiments confirmed the presence of the deposited material, but unambiguous information on the structural changes upon water sorption could not be discerned. The results (Figures S3 and S4, Supporting Information) together with detailed discussion are presented in the Supporting Information on pages 2–3. Despite the lack of PXRD evidence, we assume that the films obtained by sequential growth contain the same material in terms of crystal structure as the films obtained by the physical deposition of pre-formed nanocrystallites, and the two types of films differ only in morphology (grain size and density). This assumption is evidenced by magnetic studies results described in Section 2.3.

2.2. Sorption Studies

For the micrometric films deposited from suspension we studied water sorption by the gravimetric dynamic vapor sorption (DVS) method in comparison to the bulk samples. The NiCr and NiFe networks were obtained as several pseudopolymorphs, including fully hydrated and anhydrous forms, as well as intermediate hydrates. The fully hydrated forms, containing $22.5H_2O$ are isomorphic. The intermediate hydrates differ in structure and contain different amount of crystallization water: $16H_2O$ for NiCr and $12H_2O$ for NiFe. For the anhydrous forms the structure was not established, though both NiCr and NiFe show similar PXRD patterns. For both networks there are marked differences in magnetic behavior between each of the three forms. The water sorption isotherms for bulk microcrystalline samples measured at 25 °C show stepwise water intake (Figure S5, Supporting Information). For NiCr water sorption takes place in two sharp steps at 10% and 80% RH, with an intermediate, less pronounced step at 30% RH. The mass changes suggest the presence of three hydrates containing

10–$12H_2O$, 13–$16H_2O$, and 22.5–$23H_2O$, respectively. The desorption process occurs in two steps at about 60% and 10% RH, without the presence of the 10–$12H_2O$ hydrate, which results in an irregular wide hysteresis. The two sharp hydration/dehydration steps implicate structural transformations observed earlier in PXRD studies for bulk materials (Figure S4, Supporting Information),[19] in which the presence of the 10–$12H_2O$ hydrate was not detected, most probably due to its narrow stability range. For the NiFe network the water sorption isotherm shows a sharp initial mass increase below 10% RH, followed by gradual increase with two small steps at about 50% and 90% RH. The total mass increase of 24% corresponds to the intake of $16H_2O$, indicating that the fully hydrated form cannot be obtained by exposure to high humidity conditions, but only by immersion in water. The desorption process begins gradually, with a small indistinct step at 30% RH and the final sharp water release step at 10% RH. The lower water intake and prolonged steps in the NiFe isotherm confirm the higher stability of the low water content hydrate $NiFe \cdot 12H_2O$. It also indicates the possible existence of the $NiFe \cdot 16H_2O$ hydrate, which was not observed in solvatomagnetic studies, as most likely it is difficult to stabilize due to the gradual character of the sorption process and wide isotherm hysteresis.

The sorption properties of the thin films deposited by adsorption from suspension resemble those of bulk samples (Figure S5, Supporting Information). Due to the large mass of the substrate in comparison to the deposited material, the relative mass change observed in the sorption experiments on films is only about 1%, which is more than 20 times lower than for the bulk samples. Over the whole humidity range the mass changes are more gradual in films than in the bulk samples. It may be connected with water sorption by the substrate, the hydrophilicity of which was modified by the PDADMAC catiopolymer. At high humidity conditions surface sorption effects are visible: the mass increases sharply above 90% RH and decreases in the desorption cycle following almost the same line. For the NiCr film the sorption and desorption steps occur at the same RH as for the bulk sample. For NiFe second sorption step is shifted from 50% to 65% RH. This effect may be the indication that the adhesion to the substrate surface hinders structural changes in the deposited material.

Due to the small amount of the deposited material, for the films obtained by the sequential growth the mass changes upon sorption were too small to be detected in the DVS gravimetric method, which excluded the possibility of sorption characterization.

2.3. Solvatomagnetism

The magnetic properties of the NiCr and NiFe networks depend on the number of lattice water molecules present in their microporous structure.[19] All pseudopolymorphs show metamagnetic character, typical for layered structures, but with different critical field of metamagnetic transition. The critical temperature of long-range magnetic order and the presence and size of the magnetic hysteresis also varies between different forms. The aim of our studies was to evaluate the solvatomagnetic behavior of the thin films in comparison to
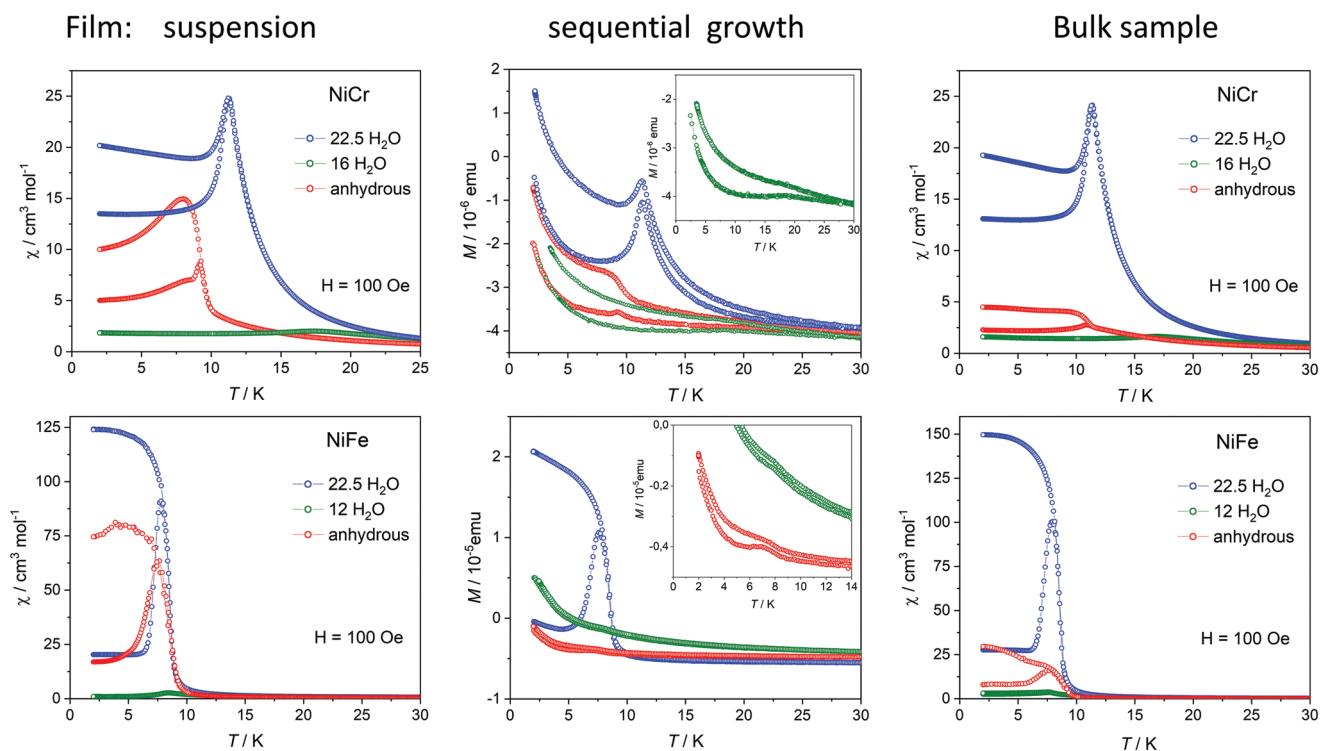
ADVANCED
SCIENCE NEWS
www.advancedsciencenews.com

ADVANCED
MATERIALS
INTERFACES
www.advmatinterfaces.de

Figure 4. ZFC-FC plots for two types of thin films and bulk samples of the $\{[Ni^{II}(cyclam)]_3[M^{III}(CN)_6]_2 \cdot nH_2O\}_n$ (M = Cr, Fe) networks.

the bulk samples. Both bulk and thin film samples for magnetic measurements were stabilized inside the DVS apparatus at the appropriate humidity conditions or covered with water and sealed in polyethylene bags to ensure the stability of the target pseudopolymorphic forms. Due to small amount of the deposited material the signal observed in the magnetometric measurements was very low and additionally impeded by a relatively large diamagnetic contribution of the substrate. The net effect of temperature-dependent low paramagnetic signal and temperature-independent strong diamagnetic signal at certain conditions oscillated around zero causing low measurement accuracy. To counteract this problem, for the thin films deposited from suspension we used additional straws placed inside the straw holder above and below the sample (Figure S6, Supporting Information) to outweigh the diamagnetic contribution of the substrate and ensure the positive signal throughout the measurements. This method also allowed us to measure the signal for the PET/ITO substrate itself and subtract it from that of the film samples. By scaling the saturation magnetization values at 1.8 K and 7 T to that of the bulk samples we estimated the amount of the deposited material at about 200 μg per 1 cm². For the thin films obtained by sequential growth the procedure described above did not give satisfactory results and therefore we present below the raw measurement data with prevalent diamagnetic contribution of the substrate and therefore negative signal over most of the temperature range.

The solvatomagnetic properties of the bulk samples were originally characterized by DC magnetic susceptibility at 1000 Oe in the 2–300 K temperature range, magnetization at 1.8 K in the −5 to 5 T field range and AC susceptibility. We appended this characterization by the ZFC/FC measurements

at 100 Oe, which proved to be the most sensitive method for the assessment of the magnetic properties of the thin films. For the anhydrous and fully hydrated forms of the bulk samples of both networks the ZFC/FC curves show bifurcation at about 11 K (NiCr) or 8 K (NiFe), indicating the onset of long range magnetic order (**Figure 4**, right). For the intermediate hydrates the ZFC/FC curves overlap below the maximum at 16.6 K (NiCr) or 7.7 K (NiFe). The ZFC/FC maxima and bifurcation points correlate well with the critical temperatures established from the AC susceptibility measurements (**Table 1**).

The ZFC/FC profiles are consistent with the magnetization versus field measurements at 1.8 K (**Figure 5**). The widest magnetic hysteresis and the largest separation between the ZFC/FC branches are observed for NiFe·22.5H₂O. The anhydrous NiFe form shows narrower hysteresis with lower remanence, which coincides with lower susceptibility at 1.8 K and smaller

Table 1. Comparison of ZFC/FC maxima and bifurcation points ($T_{ZFC/FC}$) for films and bulk samples with critical temperatures (T_c) derived from AC susceptibility for bulk samples.

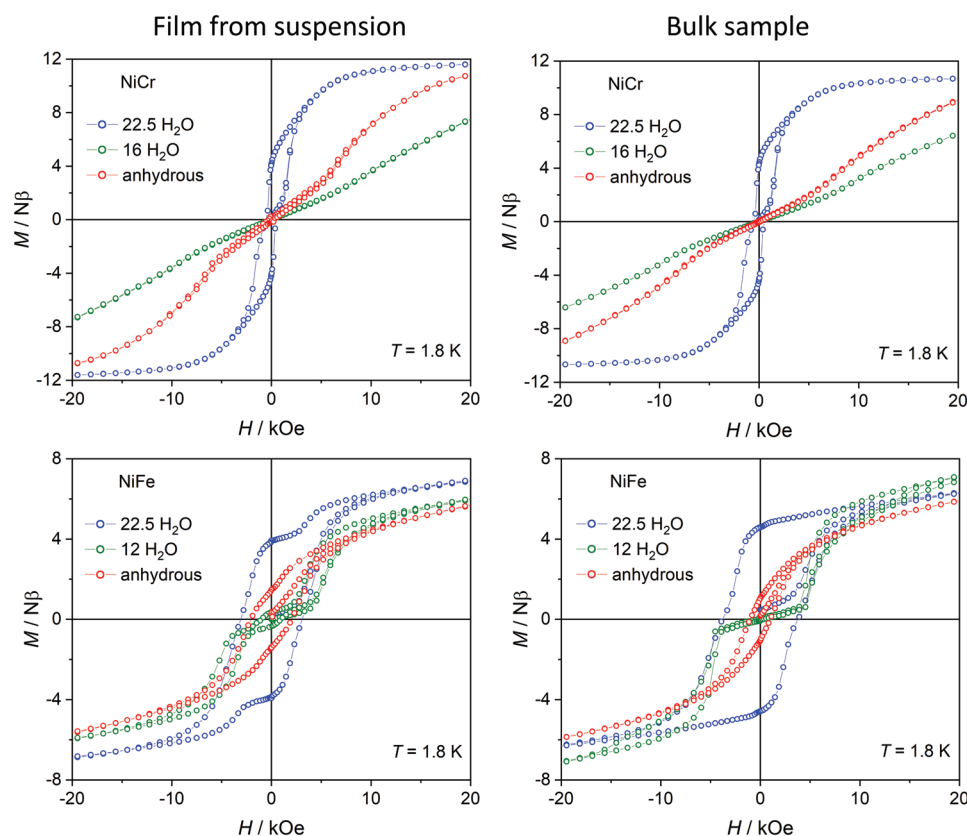| Compound	Film: suspension $T_{ZFC/FC}$ [K]	Sequential growth $T_{ZFC/FC}$ [K]	Bulk sample T_c [K]	Bulk sample $T_{ZFC/FC}$ [K]
NiCr·22.5H₂O	11.2	11.3	11.8	11.3
NiCr·16H₂O	17.3	18.4	18.0	16.6
NiCr (anhydr.)	9.1	9.2	11.0	11.4
NiFe·22.5H₂O	7.8	7.6	8.4	8.0
NiFe·12H₂O	7.4	8.0	8.3	7.7
NiFe (anhydr.)	8.4	7.0	8.6	7.6

Figure 5. Magnetization versus field at 1.8 K for thin films obtained by physical deposition and for bulk samples of the $\{[Ni^{II}(cyclam)]_3[M^{III}(CN)_6]_2 \cdot nH_2O\}_n$ (M = Cr, Fe) networks.

separation of the ZFC/FC branches. For $NiCr \cdot 22.5H_2O$ the ZFC/FC bifurcation point coincides with the maximum, which is connected with the metamagnetic character of the network, reflected also in the butterfly-like shape of the hysteresis. The anhydrous NiCr form shows very narrow hysteresis (not noticeable in the scale of Figure 5) with remanence of 0.05 Nβ, which corresponds to the maximum FC susceptibility of 5 cm^3 mol^{-1}. The intermediate hydrates show markedly higher critical field of metamagnetic transition than the other two forms of each network (**Table 2**). Magnetization of $NiCr \cdot 16H_2O$ is fully reversible, while for $NiFe \cdot 12H_2O$ a butterfly-shaped hysteresis is observed, which practically closes below 4000 Oe. These char-

acteristics are consistent with antiferromagnetic order and low susceptibility values observed at 100 Oe in the ZFC/FC experiments.

2.3.1. Films Obtained by Physical Deposition

The ZFC/FC characteristics of the micrometric-scale thin films obtained by deposition from suspension (Figure 4, left) for the intermediate hydrates and fully hydrated forms closely resemble those of the bulk materials. The maxima for $NiCr \cdot 16H_2O/NiFe \cdot 12H_2O$ and bifurcation points for $NiCr \cdot 22.5H_2O/NiFe \cdot 22.5H_2O$ appear at nearly the same temperatures (Table 1), with similar extent of separation of the ZFC/FC branches. These similarities are also reflected in the M(H) measurements (Figure 5), where comparable values of the critical fields of metamagnetic transition, remanence and coercivity are observed (Table 2). There is, however, a step-like irregularity in the shape of the $NiFe \cdot 22.5H_2O$ hysteresis, which together with slightly lower remanence and coercivity, indicates that the transformation from the intermediate hydrate to the fully hydrated form may not be complete in the thin film. The transition from $NiFe \cdot 12H_2O$ to $NiFe \cdot 22.5H_2O$ is accompanied by 17% increase in volume, while in the $NiCr \cdot 16H_2O$ to $NiCr \cdot 22.5H_2O$ transformation the volume increases only by 9%. Moreover, in contrast to $NiCr \cdot 22.5H_2O$, the fully hydrated $NiFe \cdot 22.5H_2O$ form could not be achieved in the bulk sample

Table 2. Critical field of metamagnetic transition (H_{cr}), magnetic remanence (M_{rem}) and coercivity (H_c) for films obtained from suspension and for bulk samples.

Compound	Film from suspension			Bulk sample		
	H_{cr} [Oe]	H_c [Oe]	M_{rem} [Nβ]	H_{cr} [Oe]	H_c [Oe]	M_{rem} [Nβ]
$NiCr \cdot 22.5H_2O$	1480	538	4.1	1480	543	4.3
$NiCr \cdot 16H_2O$	9250	–	–	9250	–	–
NiCr (anhydr.)	6690	–	–	7500	–	–
$NiFe \cdot 22.5H_2O$	3910	3091	3.9	4535	3791	4.6
$NiFe \cdot 12H_2O$	5218	–	–	5206	–	–
NiFe (anhydr.)	2311	2036	1.5	1874	1012	1.06

2201834 (6 of 9)

**ADVANCED
SCIENCE NEWS**

www.advancedsciencenews.com

**ADVANCED
MATERIALS
INTERFACES**

www.advmatinterfaces.de

at 96% RH, but required soaking in water. It seems probable that in the case of the NiFe network adhesion to the substrate surface and close packing of the nano-crystallites prevent structural transformation in part of the deposited material. The step-like anomaly in the NiFe·22.5H$_2$O hysteresis appeared in repeated measurements and could not be eliminated by prolonged soaking in water. The magnetic behavior of the anhydrous films is slightly different than that of the corresponding bulk samples. The bifurcation points appear at slightly different temperatures (Table 1) and the ZFC/FC branches are further apart (Figure 4), which is also reflected in wider magnetic hysteresis for both NiCr and NiFe (Figure 5, Table 2). The dehydration process affects the structure in two ways: it eliminates the water-mediated H-bonds and causes deformation of the CN-bridged coordination skeleton. Although the structure of the anhydrous forms was not established, we may assume that the second process involves considerable change in volume and may be affected by adhesion forces in thin films, causing differences in magnetic behavior. The transition between fully hydrated forms and intermediate hydrates is fully reversible, which was checked by repeated magnetic measurements. Although dehydration of the films was found reversible in water sorption (DVS) experiments at 25 °C, this reversibility was not confirmed by magnetic measurements. We suppose that the strain imposed by the volume changes upon sorption coupled with the incommensurable thermal expansion of the substrate and the deposited material, experienced by the samples upon temperature changes during magnetic measurements, causes the disintegration of the films.

2.3.2. Films Obtained by Sequential Growth

The magnetic characterization of the nanometric-scale thin films obtained by sequential growth is based on the ZFC/FC measurements. As described above, the small amount of the deposited material and large diamagnetic contribution of the substrate considerably hindered magnetometric measurements, which could be additionally affected by the presence of the conducting gold layer. The M(H) measurements, burdened with low accuracy, could not be interpreted. In order to avoid loss of information we did not attempt any data correction and in the middle part of Figure 4 we present raw results of the ZFC/FC measurements. Due to the diamagnetic contribution of the substrate the measured magnetic moment is for the greater part negative, reaching positive values only for selected forms at low temperatures. The ZFC/FC branches do not entirely overlap above the ordering temperatures. Similar splitting appears in the measurements of gold sputtered PET/ITO substrate and therefore we assume that this effect is not connected with the deposited material. Despite this splitting the bifurcation points can be clearly identified from the different trends of the ZFC/FC curves. The results obtained for the NiCr film closely resemble those for the bulk sample. The anhydrous form shows bifurcation at about 9 K with an upward trend of the FC curve. For the fully hydrated form the bifurcation point below the maximum and wide separation of the ZFC/FC branches is observed. The intermediate hydrate shows an indistinct maximum around 18 K, and although the ZFC/FC

branches are split, they follow the same trend, which allows us to attribute the splitting to the substrate effects. Notably, the maxima and bifurcations, which vary between different forms of the NiCr network appear at nearly the same temperatures as in the bulk material. For the NiFe network the ordering temperatures of different forms are similar, however, the ZFC/FC curves differ considerably. The fully hydrated form of the NiFe network shows large splitting and high susceptibility value for the FC branch. For the intermediate hydrate a small maximum and no bifurcation appears. For both these forms the film characteristics mirror the behavior of the bulk sample. For the anhydrous form the bifurcation point is visible, but in contrast to the micrometric film obtained from suspension, the splitting of the ZFC/FC branches is very small. We assume, that due to the adhesion forces and almost continuous character of the film obtained by sequential growth, the conversion to the anhydrous form is not complete and the observed signal comes from the mixture of two phases: the anhydrous one and the intermediate hydrate. Similarly to the films obtained from suspension, the films from sequential growth show full reversibility of the transition between fully hydrated forms and intermediate hydrates, but the anhydrous forms cannot be rehydrated.

3. Conclusion

We prepared thin films of two hybrid CN-bridged coordination networks {[Ni^{II}(cyclam)]$_3$[Cr^{III}(CN)$_6$]$_2$·nH$_2$O}$_n$ (NiCr) and {[Ni^{II}(cyclam)]$_3$[Fe^{III}(CN)$_6$]2·nH$_2$O}$_n$ (NiFe). By applying two different deposition methods: adsorption of nano-sized crystallites from water suspension and sequential growth of the coordination network on the substrate surface we obtained films differing in thickness and morphology. By the physical deposition method via dip-coating from suspension of pre-formed compounds, films of 1–2 μm thickness composed of crystallites of 50–200 nm size were obtained. By the chemical deposition method of in situ formation of the coordination polymer on the substrate, achieved by anchoring the [Ni(cyclam)]$^{2+}$ building block to the gold-sputtered surface followed by sequential dipping in anionic and cationic building blocks solutions, uniform thin films of 100–500 nm thickness were fabricated. Both types of films retain the solvatomagnetic properties of bulk samples changing magnetic properties upon removal/inclusion of guest water molecules. Our findings open up the possibility of fabrication of humidity-driven sensors with memory effect based on magnetic coordination polymers. Moreover, we have shown that not only Prussian blue analogues but also hybrid CN-bridged networks containing organic ligands can be obtained as highly uniform thin films, which may facilitate the utilization of the functional potential of this versatile group of coordination polymers.

4. Experimental Section

Materials: [Ni(cyclam)(NO$_3$)$_2$] was obtained by following the literature method.[47] Bulk samples of [Ni(cyclam)]$_3$[M(CN)$_6$]$_2$ · nH$_2$O (M = Cr, Fe) used in the reference sorption and magnetic measurements were synthesized as described earlier.[19] Other reagents were commercially available and used without further purification.

**ADVANCED
SCIENCE NEWS**

www.advancedsciencenews.com

**ADVANCED
MATERIALS
INTERFACES**

www.advmatinterfaces.de

Dip-Coating Deposition of NiCr and NiFe Thin Films: Powder suspensions of $[Ni(cyclam)]_3[M(CN)_6]_2 \cdot nH_2O$ (M = Cr; Fe) were prepared by quick mixing water solutions of $[Ni(cyclam)](NO_3)_2$ (14 mg, 0.037 mmol in 1.5 mL of H_2O) and $K_3[M(CN)_6]$ (7 mg, 0.02 mmol in 1.5 mL of H_2O). The precipitated powders were then washed several times with deionized water by centrifugation and decantation in order to remove other reagents. The films were fabricated on the PET substrate coated with ITO (resistance: 10–14 Ohm sq^{-1}), modified by immersion for 1 h in an aqueous solution of PDADMAC; 1%, rinsed with deionized water and dried in air. The thin films were deposited with the aid of a KSV Nima dip-coater at room temperature. In a single cycle a solid support was immersed in the constantly stirred water suspension of NiCr or NiFe for 30 s, which was followed by a 30 s drying step. The process of dip-coating deposition of NiCr and NiFe as thin films was composed of 25 cycles.

Sequential Growth of NiCr and NiFe Thin Films: The PET/ITO substrate was covered on one side with gold by sputtering in vacuum, then cleaned by immersion in hydrochloric acid (5%) for 20 min and then washed with deionized water and air dried. Fatty impurities were removed by shaking the substrate in *n*-pentane for 1 min. The cleaned substrate was immersed in an aqueous solution of 6-aminohexanethiol hydrochloride (AHT; 2×10^{-3} м) for 24–48 h under anaerobic conditions. The AHT—functionalized substrate was then rinsed with degassed water to remove non-immobilized residues of the aminothiol and air dried at ambient conditions. The substrate was then immersed in an aqueous solution of $[Ni(cyclam)(NO_3)_2]$ (50 mg, 0.13 mmol in 50 mL H_2O) for 1.5 h to ensure the anchoring of the cationic building block to the functionalized support. The sequential growth process was performed using a KSV Nima dip-coater at room temperature. Single cycle of the deposition process consisted of alternating immersion for 30 s in aqueous solutions of $[Ni(cyclam)(NO_3)_2]$ (50 mg, 0.13 mmol in 50 mL H_2O) and $K_3[M(CN)_6]$ M = Cr, Fe (50 mg, 0.15 mmol in 50 mL H_2O). Dipping the substrate in the cationic/anionic building block solution was followed by triple rinsing with deionized water in 3 different beakers for 5 s each. A total of 500 cycles were used to produce thin films of NiCr and NiFe by sequential growth deposition.

SEM Study: Morphology and thickness of the thin films were studied using HITACHI S-4700 scanning electron microscope. Grain size analysis from the SEM images was performed with the use of image processing program ImageJ 1.52a.

Sorption Study: The process of controlled sorption and desorption of water molecules was performed using a Surface Measurement System Dynamic Vapor Sorption DVS-Adventure apparatus. The experiments were carried out for bulk samples and for stacks of thin films obtained by the physical deposition from suspension. The water sorption isotherms were measured at ambient temperature (25 °C) in the range 0–96% relative humidity (RH) of water vapor with the 2% step. At each step sample weight was equilibrated ($d_m/d_t = 0.001\%$ min^{-1}).

PXRD Measurements: The diffractograms were recorded on a PANalytical X'Pert PRO diffractometer. Measurements were performed on film and substrate samples placed on a silicon zero-background holder using $K\alpha$ radiation ($\lambda = 1.5419$ Å) in a reflection mode.

Magnetic Measurements: Variable-temperature (2–30 K, applied field: 100 Oe) and field-dependent (T = 1.8 K) DC magnetization were measured using a Quantum Design MPMS 3 SQUID magnetometer. The thin films on PET/ITO/catiopolymer substrate obtained by the physical deposition from suspension were cut into 3 × 4 mm pieces and a stack of 9 pieces was sealed in a PE bag and placed in a straw holder of 5 mm diameter and immobilized by other rolled up straws cut in half (Figure S6, Supporting Information) with the applied field parallel to the surface. The magnetic properties of the PET/ITO/catiopolymer support were measured separately under the same conditions and subtracted from the raw data. Mass of the polymers deposited on the support by dip-coating technique was estimated from measurements of magnetic field dependence of magnetization at 1.8 K. The same type of straw holder was used for reference measurements of bulk samples. The thin films on PET/ITO/Au/aminothiol substrate obtained by sequential growth were cut into 6 × 5 mm pieces and a stack of 25 pieces was

sealed in a PE bag and introduced into a straw holder of 8 mm diameter with the applied field parallel to the surface. For this type of film raw measurements data are presented without any correction. All samples prior to measurements were stabilized under controlled humidity conditions. For anhydrous forms and intermediate hydrates the samples in open PE bags were kept in the DVS apparatus until constant mass at 25 °C and 0% or 60% RH, respectively, and then immediately sealed. The fully hydrated samples were sealed in water-filled PE bags.

Supporting Information

Supporting Information is available from the Wiley Online Library or from the author.

Acknowledgements

Conflict of Interest

The authors declare no conflict of interest.

Data Availability Statement

The data that support the findings of this study are available from the corresponding author upon reasonable request.

Keywords

[1] E. Coronado, *Nat. Rev. Mater.* **2020**, *5*, 87.

[2] J. S. Miller, *Chem. Soc. Rev.* **2011**, *40*, 3266.

[3] J. Ferrando-Soria, R. Ruiz-García, J. Cano, S.-E. Stiriba, J. Vallejo, I. Castro, M. Julve, F. Lloret, P. Amorós, J. Pasán, C. Ruiz-Pérez, Y. Journaux, E. Pardo, *Chemistry* **2012**, *18*, 1608.

[4] M. Feng, Z.-Y. Ruan, Y.-C. Chen, M.-L. Tong, *Chem. Commun.* **2020**, *56*, 13702.

[5] M. Reczyński, D. Pinkowicz, K. Nakabayashi, C. Näther, J. Stanek, M. Kozieł, J. Kalinowska-Tłuścik, B. Sieklucka, S. Ohkoshi, B. Nowicka, *Angew. Chem., Int. Ed.* **2021**, *60*, 2330.

[6] C. H. Woodall, G. A. Craig, A. Prescimone, M. Misek, J. Cano, J. Faus, M. R. Probert, S. Parsons, S. Moggach, J. Martínez-Lillo, M. Murrie, K. v. Kamenev, E. K. Brechin, *Nat. Commun.* **2016**, *7*, 13870.

[7] O. Sato, *Proc. Jpn. Acad. Ser. B: Phys. Biol. Sci.* **2012**, *88*, 213.

[8] P. Dechambenoit, J. R. Long, *Chem. Soc. Rev.* **2011**, *40*, 3249.

[9] O. Kahn, J. Larionova, J. V. Yakhmi, *Chemistry* **1999**, *5*, 3443.

[10] F. Pointillart, J. F. Gonzalez, V. Montigaud, L. Tesi, V. Cherkasov, B. le Guennic, O. Cador, L. Ouahab, R. Sessoli, V. Kuropatov, *Inorg. Chem. Front.* **2020**, *7*, 2322.

[11] J. Vallejo, E. Pardo, M. Viciano-Chumillas, I. Castro, P. Amorós, M. Déniz, C. Ruiz-Pérez, C. Yuste-Vivas, J. Krzystek, M. Julve, F. Lloret, J. Cano, *Chem. Sci.* **2017**, *8*, 3694.

[12] K. M. Fromm, *Angew. Chem., Int. Ed.* **2009**, *48*, 4890.

[13] S. Chorazy, J. J. Zakrzewski, M. Magott, T. Korzeniak, B. Nowicka, D. Pinkowicz, R. Podgajny, B. Sieklucka, *Chem. Soc. Rev.* **2020**, *49*, 5945.

[14] Y. Huang, S. Ren, *Appl. Mater. Today* **2021**, *22*, 100886.

[15] E. Colacio, J. M. Domínguez-Vera, M. Ghazi, J. M. Moreno, R. Kivekäs, F. Lloret, H. Stoeckli-Evans, *Chem. Commun.* **1999**, 987.

[16] S. Ferlay, T. Mallah, J. Vaissermann, F. Bartolomé, P. Veillet, M. Verdaguer, *Chem. Commun.* **1996**, 2481.

[17] B. Nowicka, M. Rams, K. Stadnicka, B. Sieklucka, *Inorg. Chem.* **2007**, *46*, 8123.

[18] B. Nowicka, M. Reczyński, M. Rams, W. Nitek, M. Kozieł, B. Sieklucka, *CrystEngComm* **2015**, *17*, 3526.

[19] B. Nowicka, M. Reczyński, M. Balanda, M. Fitta, B. Gawel, B. Sieklucka, *Cryst. Growth Des.* **2016**, *16*, 4736.

[20] J. Camarero, E. Coronado, *J. Mater. Chem.* **2009**, *19*, 1678.

[21] M. Clemente-León, H. Soyer, E. Coronado, C. Mingotaud, C. J. Gómez-García, P. Delhaès, *Angew. Chem., Int. Ed.* **1998**, *37*, 2842.

[22] M. Clemente-León, E. Coronado, Á. López-Muñoz, D. Repetto, C. Mingotaud, D. Brinzei, L. Catala, T. Mallah, *Chem. Mater.* **2008**, *20*, 4642.

[23] F. Volatron, D. Heurtaux, L. Catala, C. Mathonière, A. Gloter, O. Stéphan, D. Repetto, M. Clemente-León, E. Coronado, T. Mallah, *Chem. Commun.* **2011**, *47*, 1985.

[24] L. Hedley, L. Porteous, D. Hutson, N. Robertson, J. O. Johansson, *J. Mater. Chem. C* **2018**, *6*, 512.

[25] L. Hedley, N. Robertson, J. O. Johansson, *Electrochim. Acta* **2017**, *236*, 97.

[26] S. Ohkoshi, A. Fujishima, K. Hashimoto, *J. Am. Chem. Soc.* **1998**, *120*, 5349.

[27] C.-Y. Kao, B. Li, Y. Lu, J.-W. Yoo, A. J. Epstein, *J. Mater. Chem. C* **2014**, *2*, 6171.

[28] M. Nisula, A. J. Karttunen, E. Solano, G. C. Tewari, M. Karppinen, M. Minjauw, H. S. Jena, P. van der Voort, D. Poelman, C. Detavernier, *ACS Appl. Mater. Interfaces* **2021**, *13*, 10249.

[29] B. Bräuer, D. R. T. Zahn, T. Rüffer, G. Salvan, *Chem. Phys. Lett.* **2006**, *432*, 226.

[30] M. Cavallini, M. Facchini, C. Albonetti, F. Biscarini, *Phys. Chem. Chem. Phys.* **2008**, *10*, 784.

[31] J. Gómez-Segura, J. Veciana, D. Ruiz-Molina, *Chem. Commun.* **2007**, 3699.

[32] T. Yamamoto, Y. Umemura, O. Sato, Y. Einaga, *Sci. Technol. Adv. Mater.* **2006**, *7*, 134.

[33] F. A. Frye, D. M. Pajerowski, J.-H. Park, M. W. Meisel, D. R. Talham, *Chem. Mater.* **2008**, *20*, 5706.

[34] D. M. Pajerowski, M. J. Andrus, J. E. Gardner, E. S. Knowles, M. W. Meisel, D. R. Talham, *J. Am. Chem. Soc.* **2010**, *132*, 4058.

[35] E. Coronado, M. Makarewicz, J. P. Prieto-Ruiz, H. Prima-García, F. M. Romero, *Adv. Mater.* **2011**, *23*, 4323.

[36] N. Ozaki, H. Tokoro, Y. Hamada, A. Namai, T. Matsuda, S. Kaneko, S. Ohkoshi, *Adv. Funct. Mater.* **2012**, *22*, 2089.

[37] M. Verdaguer, G. S. Girolami, in *Magnetism Molecules to Materials V*, Wiley-VCH Verlag GmbH & Co. KGaA, Weinheim **2004**, p. 283.

[38] M. Sawczak, R. Jendrzejewski, D. Maskowicz, Y. Garcia, A. C. Ghosh, M. Gazda, J. Czechowski, G. Śliwiński, *Eur. J. Inorg. Chem.* **2019**, *2019*, 3249.

[39] W.-P. Ma, B. Yan, *Dalton Trans.* **2020**, *49*, 15663.

[40] S. Cobo, G. Molnár, J. A. Real, A. Bousseksou, *Angew. Chem.* **2006**, *118*, 5918.

[41] W. Sas, D. Pinkowicz, M. Perzanowski, M. Fitta, *Materials* **2020**, *13*, 3029.

[42] D. Mitcov, A. H. Pedersen, M. Ceccato, R. M. Gelardi, T. Hassenkam, A. Konstantatos, A. Reinholdt, M. A. Sørensen, P. W. Thulstrup, M. G. Vinum, F. Wilhelm, A. Rogalev, W. Wernsdorfer, E. K. Brechin, S. Piligkos, *Chem. Sci.* **2019**, *10*, 3065.

[43] D. S. Krylov, S. Schimmel, V. Dubrovin, F. Liu, T. T. N. Nguyen, L. Spree, C. Chen, G. Velkos, C. Bulbucan, R. Westerström, M. Studniarek, J. Dreiser, C. Hess, B. Büchner, S. M. Avdoshenko, A. A. Popov, *Angew. Chem., Int. Ed.* **2020**, *59*, 5756.

[44] C. Chen, L. Spree, E. Koutsouflakis, D. S. Krylov, F. Liu, A. Brandenburg, G. Velkos, S. Schimmel, S. M. Avdoshenko, A. Fedorov, E. Weschke, F. Choueikani, P. Ohresser, J. Dreiser, B. Büchner, A. A. Popov, *Adv. Sci.* **2021**, *8*, 2000777.

[45] M. Fitta, H. Prima-Garcia, P. Czaja, T. Korzeniak, M. Krupiński, M. Wojtyniak, M. Bałanda, *RSC Adv.* **2017**, *7*, 1382.

[46] D. M. Pajerowski, J. E. Gardner, M. J. Andrus, S. Datta, A. Gomez, S. W. Kycia, S. Hill, D. R. Talham, M. W. Meisel, *Phys. Rev. B* **2010**, *82*, 214405.

[47] D. E. Berry, S. Girard, A. McAuley, *J. Chem. Educ.* **1996**, *73*, 551.

2201834 (9 of 9)